# Molecular Dynamic Investigations of the Mutational Effects on Structural Characteristics and Tunnel Geometry in CYP17A1

Ying-Lu Cui, Qing-Chuan Zheng,* Ji-Long Zhang, Qiao Xue, Yan Wang, and Hong-Xing Zhang*

State Key Laboratory of Theoretical and Computational Chemistry, Institute of Theoretical Chemistry, Jilin University, Changchun, Jilin 130023, P. R. China

S *Supporting Information*

ABSTRACT: Cytochrome P450 (CYP) 17A1 is a dual-function monooxygenase with a critical role in the synthesis of many human steroid hormones. The enzyme is an important target for the treatment of breast and prostate cancers that proliferate in response to estrogens and androgens. Despite the ample experimental mutagenesis data, the molecular origin and the structural motifs for the enzymatic activities deficiencies have not been rationalized at the atomic resolution. To this end, we have investigated the effects on structural characteristics and tunnel geometry upon single

point mutations in CYP17A1. The MD simulation results combined with PMF calculations and MM-GBSA calculations render an "access mechanism" which encapsulates the effects of mutations on the changes in both structural flexibility and tunnel dynamics, bridging the gap between the theory and the experimentally observed results of enzymatic activity decrease. The underlying molecular mechanism of the heterogeneities in open/closed conformational changes, as well as the wider opening of their respective major tunnels between wt17A1 and two mutants, may be attributed to the closer distances of hydrophobic residues or the disruption of a hydrophobic core. The knowledge of ligand binding characteristics and key residues contributions could guide future experimental and computational work on CYPs so that desirable changes in their enzymatic activities may be achieved. The present study provides important insights into the structure−function relationships of CYP17A1 protein, which could contribute to further understanding about 17-hydroxylase deficiencies and may also improve the understanding of polycystic ovary disease.
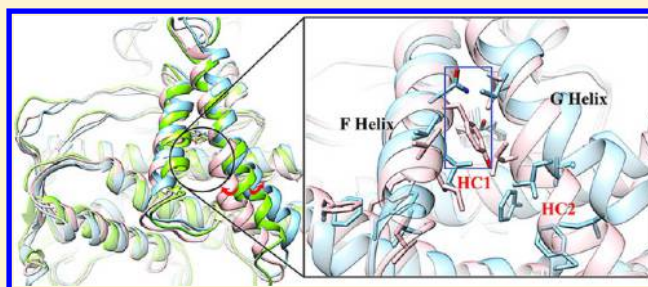
INTRODUCTION

The P450s (CYPs) are ubiquitous heme-containing mixed function oxygenases that catalyze the hydroxylation of non-activated hydrocarbon reactions, dealkylation, epoxidation, and dehydrogenation reactions involved in the oxidative metabolism.[1−3] They play a critical role in the metabolism of endogenous and exogenous substrates like drugs and environmental chemicals.[4,5] Members of this family including CYP3A4, CYP2D6, CYP2C9, CYP2C19, CYP2E1, and CYP1A2 are medically significant, which account for the oxidation of approximately 90% of drugs currently on the market.[6,7]

CYP17A1 (also known as cytochrome P450c17) is a dual-function monooxygenase with a vital role in both adrenal and gonadal steroidogenesis in mammals.[8,9] As a key enzyme in the steroidogenic pathway, the 17α-hydroxylase/17,20-lyase activities of CYP17A1 are required for the biosynthesis of cortisol in the adrenal zona fasciculata and the generation of androgenic steroids and estrogens in the adrenal zona reticularis and in gonads.[10−12] Recently, Emily E. Scott et al.[8] determined the crystal structure of CYP17A1 with prostate cancer drugs abiraterone to elucidate the structural features of this enzyme. Abiraterone is a potent, selective, and irreversible inhibitor of CYP17, which has been shown to be safe, with promising

antitumor activity in chemotherapy-naive patients with castration-resistant prostate cancer (CRPC).[13,14]

To date, more than 50 CYP17A1 mutations have been identified. The biochemical effects of two clinical mutations (Y201N and E305G) can be mostly realized by examining the CYP17A1 structure. Y201 and E305 locate proximally with abiraterone, and E305 forms a hydrogen bond to N202 in the active site from the crystal structure, indicating a role in ligand positioning and may indirectly affect the channels for ligand access or product release. Both mutations Y201N and E305G are identified in patients with enzymatic activities deficiencies.

Despite the mutation experiments on CYP17A1 protein, the molecular origin and the structural motifs to explain the decreased enzymatic activities have not been rationalized at the atomic-level. To this end, we have investigated the atomic-level structural characterization of wild type CYP17A1 and its two important mutants (Y201N and E305G). The aims of this work are to answer the following questions: i) What are the structural similarities and differences between Y201N and E305G mutant proteins with respect to the wild type CYP17A1? ii) What are the molecular motifs corresponding to the experimentally
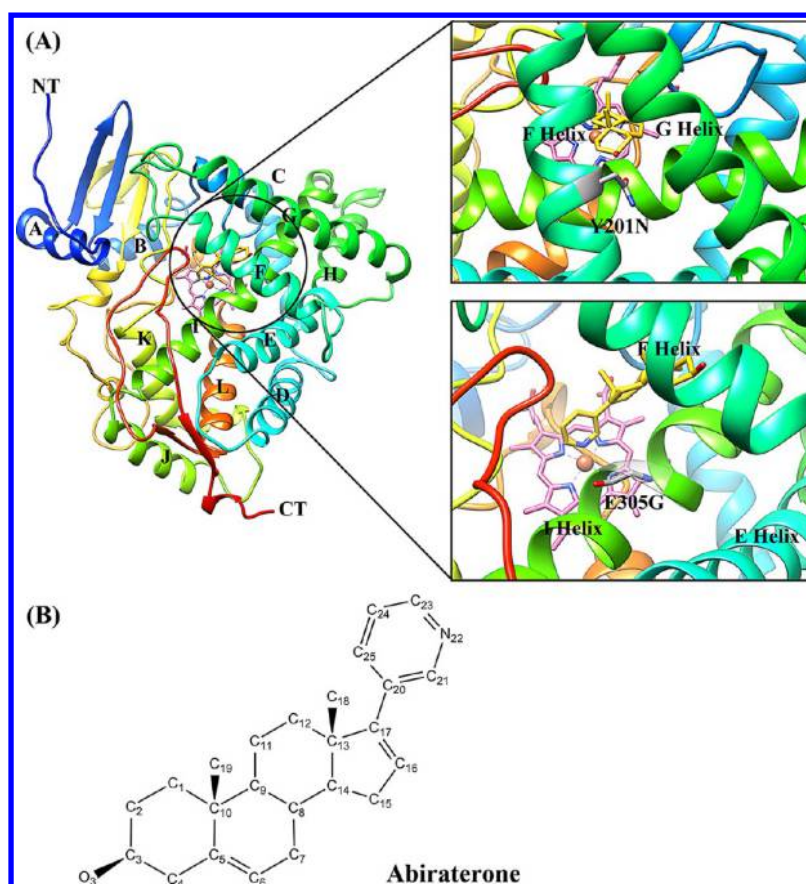
Figure 1. (A) The overall structure of CYP17A1, colored from N-terminal (blue) to C-terminal (red). The residues mutated in this study are also represented in gray sticks. (C, O, and N are gray, red, and blue, respectively.) (B) Structure of abiraterone.

observed decreased enzymatic activities? iii) What are the mutations effects on possible access tunnels and ligand binding? On the basis of MD simulations[15] and SMD simulations,[16] we present an "access mechanism" which encapsulates the effects of mutations on the changes in both structural flexibility and tunnel dynamics, bridging the gap between the theory and the experimentally observed results of enzymatic activity changes. Our work provides detailed atomistic insights into the structure−function relationships of CYP17A1 and its two mutants in dynamic motions and could contribute to further understanding about 17-hydroxylase deficiencies and may also improve the understanding of polycystic ovary disease.

COMPUTATIONAL METHODS

Preparation of the Structure. Initial structure for wild type CYP17A1 in complex with abiraterone (wt17A1) was taken from Protein Data Bank (PDB ID: 3RUK).[8] The starting structures of two mutants were modeled using Discovery Studio 3.0[17] based on the X-ray structure of wt17A1. Hydrogen atoms were subsequently added to the complex structure with the t-Leap procedure of AMBER 11.[18] All crystal water molecules were kept during the MD simulations.[19] The force field parameters of abiraterone complexed with heme were supplied by AMBER11 with electrostatic potential fitting procedure and Gaussian09 software.[20] Structural optimization of abiraterone complexed with heme was conducted using B3LYP combined with an LACVP basis set on Fe and 6-31G basis set on the others using the Gaussian09 software. RESP fitting procedure was used for charge derivation based on the

optimal geometry. The force field parameters also refer to previous QM/MM simulations.[21−23]

Molecular Dynamics Simulations. MD simulations for wt17A1 and two mutants including energy minimization were carried out using AMBER 11[18] software package and the ff99SB force field.[24] To keep the whole systems neutral, chloride ions (Cl^-) were added using the t-Leap procedure of AMBER 11 based on a coulomb potential grid. Each system was then solvated with the TIP3P water model in a truncated octahedron box with a 10 Å distance around the solute. The whole systems were submitted to 2000 steps of steepest decent minimization followed by 3000 steps of conjugate gradient minimization. Subsequently, the systems were heated from 0 to 300 K in 300 ps by a Langevin dynamics with the collision frequency of 1 ps^{-1}. Then, the systems went through 500 ps equilibrium MD simulations. Finally, a total of 50 ns were simulated for each system under NPT ensemble condition using periodic boundary conditions and particle-mesh Ewald (PME) for long range electrostatics. Short range interactions were cut off at 12 Å, and bonds involving hydrogen were held fixed using SHAKE. The time step was set to 2 fs. The cluster analysis of the protein conformations is performed using the average linkage as the clustering algorithm and backbone atom RMSD as the distance metric. It can be summarized as follows: under the average linkage algorithm, the distance from one cluster to another is defined as the average of all distances between individual points of the two clusters. At each iteration step, the two closest clusters are merged. This merging continues until the desired number of clusters is obtained (here is 5). The representative structures of the clusters with highest occur-
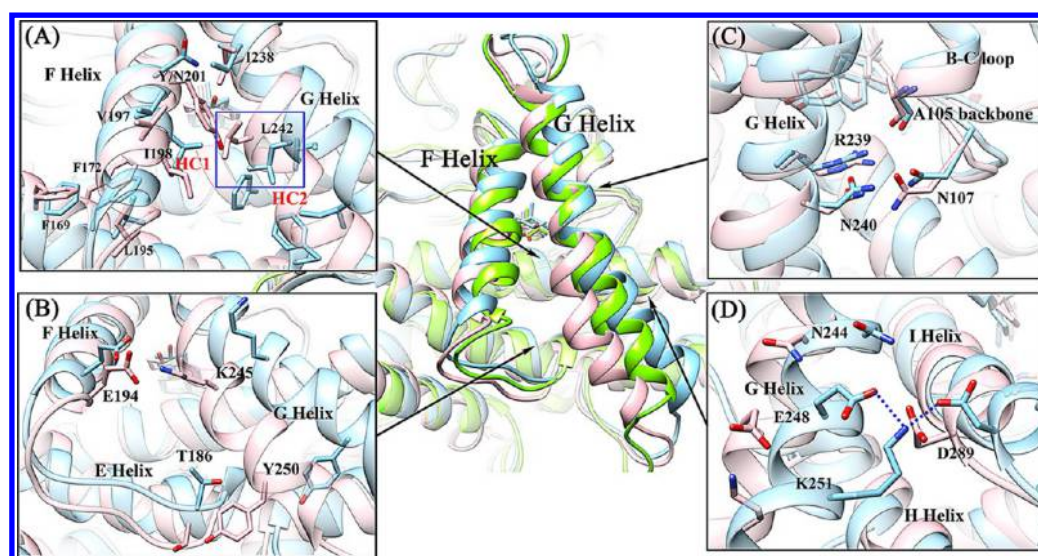
3309

dx.doi.org/10.1021/ci400553w | *J. Chem. Inf. Model.* 2013, 53, 3308−3317

Figure 2. Representative structures of wt17A1 (green), Y201N (blue), and E305G (pink). All structures are superposed on the representative structure of wt17A1. Crucial residues which may mediate the structural changes of F, G helices for two mutants are shown in stick representation. (A) The hydrophobic interactions between F and G helices, as well as F and E helices in two mutants; (B) The salt bridges formed between E194 of F helix and K245 of G helix and between T186 of E-F loop and Y250 of G helix; (C) The hydrogen bonding network including R239, N240 of G helix and A105, N107 of the B−C loop; (D) The new salt bridge network including E248, K251 of G helix and D289 of I helix in Y201N mutant.

rences for wt17A1, Y201N, and E305G were chosen to present the structural information, respectively. All of the figures were created with PyMOL and Chimera.[25,26]

Free Energy Calculations. The MM-GB/SA methods implemented in AMBER 11[18] was applied to calculate the binding free energy between the ligand with the enzyme.[27] The binding free energy (ΔG_{bind}) in MM-GB/SA between a ligand (L) and a receptor (R) to form a complex RL was calculated as

$$\Delta G_{bind} = G_{complex} - (G_{receptor} + G_{ligand}) \quad (1)$$

$$G = E_{MM} + G_{sol} - TS \quad (2)$$

$$E_{MM} = E_{int} + E_{ele} + E_{vdw} \quad (3)$$

$$G_{sol} = G_{GB} + G_{SA} \quad (4)$$

In eq 2, the E_{MM}, G_{sol}, and TS represent molecular mechanics component in gas phase, the stabilization energy due to solvation, and a vibrational entropy term, respectively. E_{MM} is given as a sum of E_{int}, E_{ele}, and E_{vdw} which are internal, Coulomb and van der Waals interaction terms, respectively. Solvation energy, G_{sol}, is separated into an electrostatic solvation free energy (G_{GB}) and a nonpolar solvation free energy (G_{SA}). The former can be obtained from the Generalized Born (GB) method. The latter is considered to be proportional to the molecular solvent accessible surface area (SASA).[28] The binding free energies were obtained by averaging over the values calculated for 20000 snapshots from the last 40 ns of the trajectories at 2 ps intervals for the complex structure.

New Analysis of Access Tunnels. CAVER is a software tool widely used for the identification and characterization of transport pathways. Herein a new version CAVER 3.0[29,30] was used to find the possible access tunnels, which thread from the surface to the active site of the enzyme, enabling automatic analysis of large ensembles of protein conformations. The ligands above the heme group were chosen as the starting points for tunnel searching. 200 snapshots of each MD simulation trajectory were extracted at an interval of 200 ps.

The probe radius and the clustering threshold were set to 1.0 and 3.5, respectively. Default settings for other parameters were used throughout the calculations. The maximum number of tunnel clusters that will be reported was set to 999. Then the tunnels were visualized using PyMOL.[25]

SMD Simulations and PMF Calculation. In the present study, multiple SMD simulations were performed using Amber 11.[18] In the SMD simulations, the reaction coordinate was specified as the distance between the iron atom in the heme group and the O3 atom in abiraterone (see the atom numbers in Figure 1(B)). The reaction coordinate is termed heme(Fe)-abiraterone(O3). In the simulations, the pulling velocity was set to 10 Å/ns, which has been used for the construction of PMF profiles. Abiraterone was pulled from approximately 15.0 to 40 Å on the reaction coordinate. The initial positions of abiraterone were somewhat different in each system and indicated a stable distance in the abiraterone-bound form of three systems during the last 40 ns MD simulation, whereas the position at 40 Å indicated a distance completely pulled out of the binding site. Many researchers also have reported that 40 Å is a reasonable position.[31] A large spring constant k (k = 5000 kcal mol^{-1} Å^{-2}) was used to ensure that the pulled atoms follow the constraint closely, a condition known as the stiff spring approximation and required for an efficient application of Jarzynski's identity.[32] Jarzynski's equality was used to establish a connection between equilibrium free energies calculation and nonequilibrium processes such as SMD simulations.[32−34] In this study, a total of 20 SMD simulations of each system were performed.

■ RESULTS AND DISCUSSION

Global Protein Topologies Are Reserved upon Introduction of Single Point Mutations in CYP17A1. Initial structure for wild type CYP17A1 in complex with abiraterone (wt17A1) was taken from Protein Data Bank (PDB ID: 3RUK).[8] The starting structures of two mutants were modeled based on the X-ray structure of wt17A1 (see Figure 1).

In the 50 ns MD simulations, the root-mean-square deviations (RMSD) of all backbone atoms for three complex structures were calculated to provide an overall measure of the departure of the structures from the initial coordinates (Figure S1). It is clear that the RMSD values are convergent and the systems remain in equilibrium during the last 40 ns for all complexes. In this regard, the results demonstrate that the global structures of three proteins are relatively conserved. All subsequent conformational characteristic analysis of wt17A1, Y201N, and E305G were performed on the last 40 ns of the simulation trajectories. During the last 40 ns simulations, the backbone atoms RMSD values for all three proteins stay fairly low with the average RMSD values of 1.58 Å (standard deviation: 0.08 Å), 1.76 Å (0.14 Å), and 1.82 Å (0.08 Å) for wt17A1, Y201N, and E305G, respectively.

Another look at the plots in Figure S2 points out the structural stability of the individual elements of secondary structure. As shown in Figure S2, on average, the global secondary structure motifs are well maintained over the 50 ns simulations of wt17A1 and two mutants. On the basis of the above structural analysis, the global protein structure and the overall topology for CYP17A1 are quite reserved by Y201N and E305G mutations.

Two Mutations Increase Protein Flexibility by Local Collective Protein Motions. Although the global structures are reserved between wild type and two mutants of CYP17A1, the local structural features are quite distinctive. The heterogeneities in conformational changes between wt17A1 and two mutants are demonstrated in Figure 2.

The representative structures for three proteins based on the clustering analysis were superimposed with each other to obtain the preliminary estimation of the effect of mutations over the conformational changes of the protein. When the representative structures of two mutants are compared with the wild type structure, it is observed that F and G helices show obvious structural migrations in two mutants. F helices of both mutants are observed to move toward the C-terminal of E helix direction, whereas the differences are most evident in the repositioning of G helices for the two mutants. The outward motion of G helix for Y201N leads to a wide conformational change, which can be identified as an "open conformation" of the protein. In contrast, the movement of G helix toward the F helix forms a "closed conformation" in E305G mutant.

The underlying molecular mechanism of the heterogeneities in conformational changes between wt17A1 and two mutants may be suggested in the following explanations. We first pay attention to mutation E305G, in particular the lost interaction between residues G305 and N202. N202 has important contributions to abiraterone binding through the formation of hydrogen bonds in approximately 81.70%, 94.51%, and 81.70% frames for wt17A1, Y201N, and E305G, respectively. In wt17A1, E305 forms hydrogen bond with N202 in more than 42% frames in the simulation trajectories. For E305G, in the absence of the carboxylate side chain, I206 and N202 extend their side chains to the unfilled space adjacent to the mutational G305, leading to a series of successive movement of the residues in N-terminal of F helix. Thus the closer distances between L195, I198 of F helix and F169, F172 of E helix make the hydrophobic interactions more stable. Notably, a hydrophobic core (HC1) consists of V197, I198, Y201, I238, and L242, associating with the hydrophobic interactions between F and G helices (shown in Figure 2(A) and Figure S3(A), (B)). With the shifts of V197, I198, and Y201 toward the C-terminal

of E helix direction, I238 and L242 make movements to the F helix accordingly. Subsequently, concomitant conformational changes occur. The salt bridge formed between E194 of F helix and K245 of G helix are monitored more frequently than wt17A1 and Y201N (41.34%, 34.69%, and 30.85% for E305G, wt17A1, and Y201N, respectively), whereas a new hydrogen bond is formed between T186 of E-F loop and Y250 of G helix in E305G protein (see Table 1, Table 2, Figure 2(B), and

Table 1. Hydrogen Bonds Occupancies of Crucial Residues for wt17A1, Y201N, and E305G

	H-bond	occupied (%)		
		wt17A1	Y201N	E305G
1	E194@O−K245@H	8.90	8.62	11.26
2	V197@O−Y/N201@H	NA	17.37	NA
3	I198@O−N202@H	NA	NA	64.16
4	Y/N201@O−N202@H	NA	NA	26.14
5	Y250@O−T186@H	NA	NA	65.39
6	E/G305@O−N202@H	42.28	44.44	NA
7	A105@O−R239@H	97.36	85.53	73.68
8	N107@O−R239@H	73.78	54.51	52.49
9	N107@O−N240@H	96.68	94.23	70.31
10	N240@O-R239@H	99.55	98.02	99.51
11	N240@O−N107@H	93.25	83.17	65.13
12	E248@O−N244@H	5.14	9.84	2.55
13	E248@O−K251@H	9.59	10.85	10.34
14	D289@O−K251@H	NA	39.48	NA
15	N202@O-ARE@H6	81.70	94.51	81.70

Table 2. Salt Bridges Occupancies of Crucial Residues for wt17A1, Y201N, and E305G

	salt bridges	occupied (%)		
		wt17A1	Y201N	E305G
1	E194@O−K245@N	34.69	30.85	41.34
2	N107@O−R239@N	99.04	96.05	73.82
3	N240@O−R239@N	100.00	99.74	99.88
4	E248@O−K251@N	41.93	44.71	40.97
5	D289@O−K251@N	NA	61.98	NA

Figure S3(C)). In addition, the hydrogen bonding network including R239, N240 of G helix and A105, N107 of B−C loop holds the middle of G helix to prevent the shift (Figure 2(C) and Figure S3(D)). Overall, these factors collectively cause the movements of N-terminal of F helix and the C-terminal half of G helix toward the F helix direction.

In Y201N mutant, the absence of aromatic ring introduces substantial disruption of the hydrophobic core interactions, which decreases the stability of the native conformation. To characterize the mutation effect on the hydrophobic core disruption, we analyzed the solvent accessible surface area (SASA)[35] in connection with the cross-correlation analysis.[36] Structural compactness of HC1 along the MD simulations was assessed by SASA. Figure 3 represents the relative differences in SASA between Y201N, E305G, and wt17A1. The comparison unequivocally reveals high increase in solvent exposure for HC1 in Y201N after 4 ns. This result may indicate that hydrophobic residues of HC1 deviate from the core without the constraints of hydrophobic actions after 4 ns, and this detached state lasts for nearly 46 ns. In the wt17A1 and E305G simulations, native contacts involving this set of residues are well conserved, whereas longtime hydrophobic loss occurs in Y201N. A closer
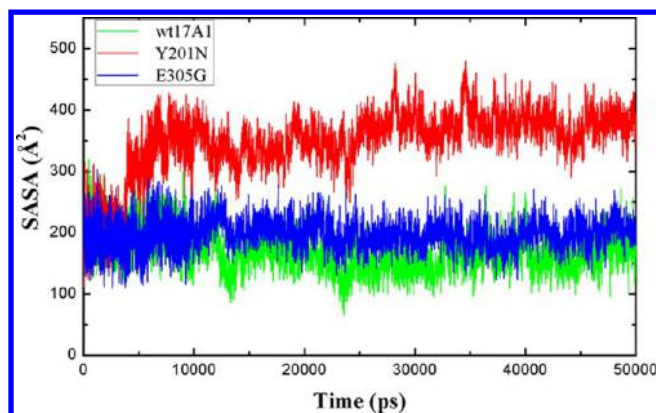
Figure 3. Variation of the solvent accessible surface area (SASA) of HC1 along MD simulations for wt17A1 (green), Y201N (red), and E305G (blue).

look at the cross-correlation analysis in Figure 4 points out details on the HC1 residues side chains movements. As shown in Figure 4, in E305G mutant, the correlation between residues in HC1 is mainly associated with V197, which is regarded as a linker between F and G helices. V197-I238, I198-I238, and V197-L242 pairs employ stronger positive correlations compared with wt17A1, whereas the Y201-L242 pair shows decreased correlation according to the upward movements by L242 to V197. However, the correlations in Y201N mutant sharply decrease between I238, L242 of G helix and the other three residues of F helix as a result of the disruption of hydrophobic core interactions. Remarkably, in a detached state, L242 distinctively rotates its side chain about 90° to participate in another hydrophobic core (HC2) which consists of F184, L243, I246, and F300 (see Figure 2(A)). With disruption of

HC1, a new salt bridge network including E248, K251 of G helix and D289 of I helix is found to be formed to "pull" the C-terminal half of G helix away from F helix. As shown in Figure 2(D) and Figure S3(E), wt17A1 and E305G mutant only display a single salt bridge between E248 and K251. To further visualize the mutation effect on the hydrophobic core disruption and hydrophobic residues movements, surfaces around F and G helices are displayed in Figure 5. As shown in Figure 5(B), Y201N mutant clearly shows a deep cavity which exposes the active site void to the solvent, correlating well with the results of SASA. While in E305G mutant, the cavity is blocked due to the shifts of hydrophobic residues in HC1.

In summary, the closer distances between hydrophobic residues or the disruption of the HC1, which associates with the hydrophobic interactions between F and G helices, can indeed be one underlying cause for the local structural motions of two mutants. However, the open and closed forms seem not to be unified to explain the common catalysis deficiencies caused by these two mutations. Accordingly, subsequent tunnels analysis, which is inferred to provide detailed characteristics of individual transport pathways and their time evolution, is used to speculate the origin for the catalysis changes in another aspect.

E305G Mutant Shows Different Major Access Tunnel Compared with Wt17A1 and Y201N Mutant. The active site of CYPs is usually isolated from the surrounding solvent as the result of the heme cofactor nearby, which is buried in the core of the enzymes. The deeply buried active site points out the question of how molecular species enter the active site from protein surface through a series of access channels prior to reaction. Thus the occurrences of tunnels in P450s are of highly
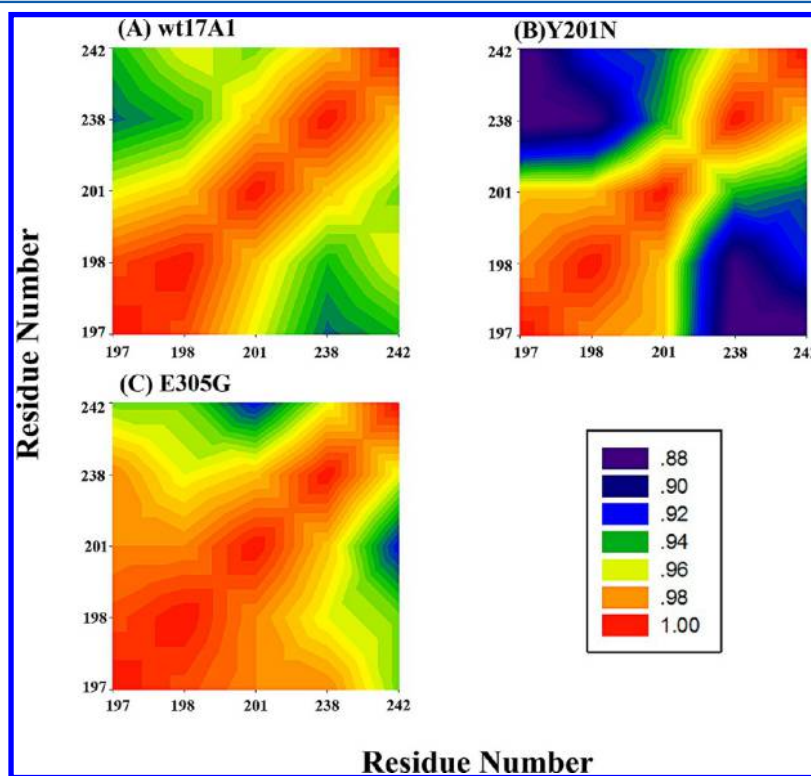

Figure 4. Cross-correlation matrices of the coordinate fluctuations for Cα atoms of (a) wt17A1, (b) Y201N, and (c) E305G proteins around their mean positions during the last 40 ns simulations. The extents of correlated motions and anticorrelated motions are labeled in different colors.
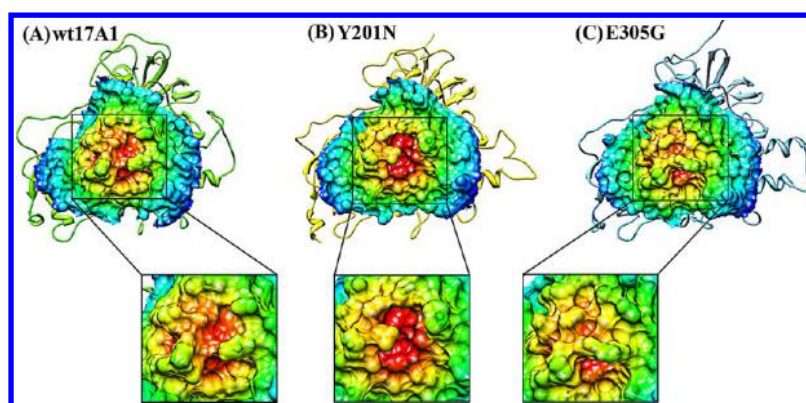
Figure 5. Molecular surfaces colored by radius from the active site for (a) wt17A1, (b) Y201N, and (c) E305G mutants.

concern for its important role in protein engineering and drug design.[37]

Multiple protein conformations were chosen from the last 40 ns MD simulations at a 200 ps interval to analyze the relevant characteristics of individual transport tunnels in three structures. The tunnels were clustered by the average-link algorithm based on the pairwise distances of the tunnels. Five top ranked tunnels of wt17A1 and two mutants identified throughout the MD simulations are all visualized in Figure 6, and the characteristics of these tunnels are summarized in Table 3.
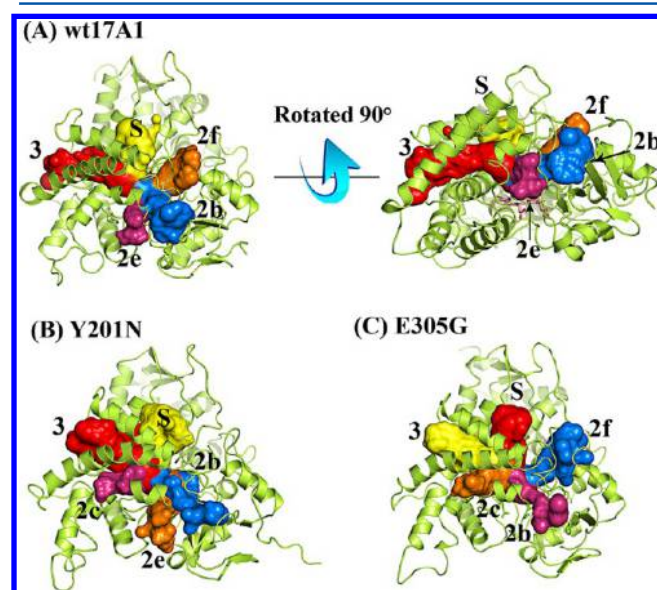

Figure 6. Five top ranked collective pathways identified throughout the molecular dynamics simulations are all depicted in one frame as pathway surfaces. Pathways following the ranking order are shown as red, yellow, blue, orange, and pink surfaces, respectively. The structures are shown in cartoon representation, whereas abiraterone and the heme group are shown in stick representations.

As shown in Figure 6, the locations of five tunnels in wt17A1 are defined as 3, S, 2f, 2b, and 2e, for Y201N mutant, there are 3, S, 2b, 2e, and 2c tunnels, whereas for E305G mutant, tunnels S, 3, 2f, 2c, and 2b have higher occurrence frequencies than other tunnels. The nomenclature for these tunnels is identified systematically by Cojocaru et al.[37] comparing to observations from MD simulations and other experimental data. Tunnel 3 and tunnel S are the dominant transport pathway in all three

Table 3

(A) Characteristics of the Top Ranked Pathways of wt17A1					
parameter			value		
pathway	3	S	2f	2b	2e
occurrence[a]	70%	56%	49%	45%	35%
mean bottleneck radius[b] [Å]	1.10	1.11	1.05	1.04	1.04
max. bottleneck radius [Å]	1.68	1.63	1.41	1.32	1.34
mean pathway length[b] [Å]	25.47	14.92	22.68	26.24	20.27
mean throughput[b,c]	0.48	0.53	0.38	0.31	0.40
(B) Characteristics of the Top Ranked Pathways of Y201N Mutant					
parameter			value		
pathway	3	S	2b	2e	2c
occurrence[a]	94%	68%	36%	11%	9%
mean bottleneck radius[b] [Å]	1.41	1.07	1.02	0.96	0.96
max. bottleneck radius [Å]	2.09	1.37	1.46	1.10	1.14
mean pathway length[b] [Å]	25.51	15.30	27.06	21.09	21.92
mean throughput[b,c]	0.53	0.50	0.24	0.39	0.38
(C) Characteristics of the Top Ranked Pathways of E305G Mutant					
parameter			value		
pathway	S	3	2f	2c	2b
occurrence[a]	87%	53%	47%	27%	12%
mean bottleneck radius[b] [Å]	1.19	1.07	1.09	1.13	0.96
max. bottleneck radius [Å]	1.78	1.55	1.49	1.60	1.21
mean pathway length[b] [Å]	19.34	26.98	22.42	19.84	26.47
mean throughput[b,c]	0.58	0.42	0.43	0.52	0.29

[a]Occupancy of snapshots in which at least one pathway with bottleneck radius ≥ 1.0 Å accounted entire snapshots. [b]Characteristics averaged over identified pathways, real values will be lower, especially for tunnel 2 subclasses, which were identified only in a small portion of snapshots. [c]The mean throughput of a give pathway, throughput = e^{-cost}.

structures. Tunnel 3, which locates between the F and G helices, is rarely observed in the top ranked tunnels of other P450s and serves as a newly dominant tunnel. The solvent tunnel (tunnel S), which runs between the E, F, and I helices and $\beta 5$ sheet, is proposed as a route for water to enter and leave the active site. However, in the present study, tunnel S is the significant transport pathway for ligands access and will be further corroborated in the steered molecular dynamics (SMD) simulations section. Tunnels 2b, 2c, 2e, and 2f are subclasses of tunnel 2. These common pathways are also observed in other cytochrome P450s[37−39] and will not be discussed in detail in the present study.

The Respective Major Tunnels Open Wider in Both Mutants According to Tunnel Dynamics. To gain a deeper
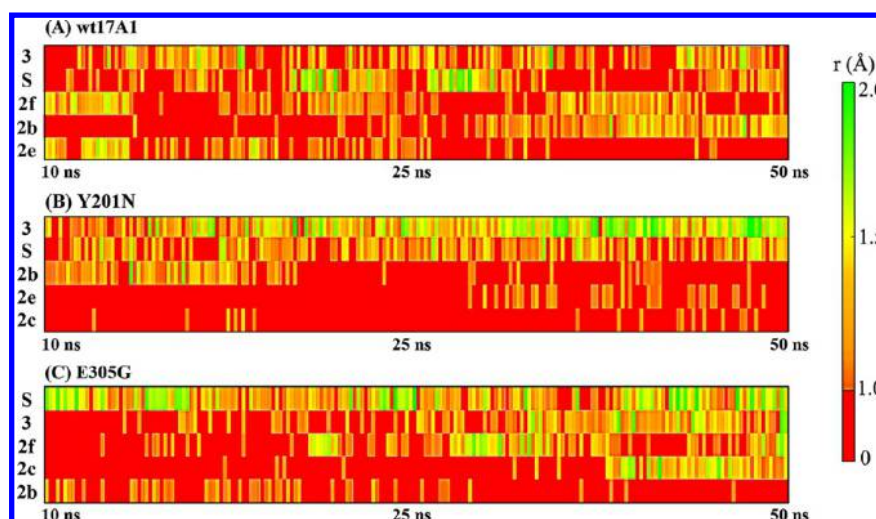
Figure 7. Time evolution correlation between the opening and closing of different pathways during the simulations. The color map ranges from very narrow (orange) to wide (green) bottlenecks. Red color indicates that no pathway with bottleneck radius ≥1.0 Å was identified for the given pathway cluster in the given snapshots.

comprehension, opening and closing motions of each tunnel are investigated. Time evolution of characteristics of individual tunnel clusters, which provides a graphical overview of bottleneck radii of these clusters are displayed in Figure 7.

As shown in Figure 7, tunnel 3 is the most frequently identified collective pathway in both wt17A1 and Y201N and has the highest maximum and mean radii of bottlenecks. It significantly opens wider in Y201N mutant, which correlates very well with the opening of F, G helices. In particular, the wider opening of tunnel 3 after about 25−40 ns in Y201N mutant simulation is associated with the increase of SASA values as shown in Figure 3. Accordingly, the disruption of the hydrophobic core interactions is suggested as a factor to facilitate the opening of tunnel 3. In E305G mutant, the amplitude of the opening of tunnel S is larger compared with other two proteins. In this regard, closed form may lead to the relative close of tunnel 3, whereas the existent other tunnel S ranks as the dominant pathway instead of tunnel 3, providing alternative route for ligands to enter the protein active site. Remarkably, both mutants show relatively more frequent opening of the major pathway (tunnel 3 for Y201N mutant and tunnel S for E305G mutant) and wider bottlenecks than the wild type protein, leading to the more exposure of ligands to aqueous solution. Thus the decreased enzymatic activities caused by Y201N or E305G mutants can be rationally associated with the more exposure of ligands which may lead to the less affinity of ligand binding. Tunnel 2 subclasses show discrete openings during the simulations, although they are only rarely identified compared with tunnel 3 and tunnel S, tunnel 2 pathways can still temporarily open for ligand access with considerable widening of the bottlenecks in some snapshots.

Tunnel Bottleneck Residues Analysis and Binding Free Energy Decomposition Calculations. To get an overview of key residues which make up individual tunnel clusters, informative characteristics of tunnel bottlenecks are obtained in Table S1. Several essential residues are observed to lie close to the tunnels, maintaining the proper protein structural flexibility or rigidity and tunnel conformation. These residues (A105, A113, F114, F172, Y/N201, N202, E203, I205, I206, L209, L214, R239, G301, A302, V304, E/

G305, T306, V366, A367, I371, V482, and V483) serve as structural elements of both tunnel 3 and tunnel S to uphold the rigidity and integrity of the protein structure and have essential impact on the tunnel geometry. In addition, I198, Y/N201, and L242 (involved in HC1), which mediate the gating of F, G helices, are the most frequent bottleneck in tunnel 3 only. This proposed structural basis of gating in the bottleneck is in agreement with the results of conformational changes mentioned above.

Table S2 lists the crucial residues which make large contributions to the ligand binding affinity for all three systems. Several hydrophobic residues, A113, F114, N202, I205, I206, R239, G301, A302, E305, T306, I371, and V483 are involved in the essential bottlenecks residues, and they also make large contributions to the ligand binding. In other CYPs, hydrophobic residues have indeed been found to locate near access tunnels to control substrate access, and they may play crucial roles in recognizing the substrate and guiding the substrate into the active site.[40,41] In the present study, the hydrophobic bottleneck residues, which lie above the active site with side chains stacking against each other, collectively form a hydrophobic cavity and provide hydrophobic interactions to play an indispensable role in the stabilization of ligands, especially A113, F114, I205, I206, A302, I371, and V483. For these hydrophobic residues with the contributions of binding free energy lower than −0.8 kcal mol^{-1}, there are primarily van der Waals effects that serve the stabilization of tunnel architecture and ligand binding. Chief among these are the side chains of A302 and I205, which make strongly favorable interactions with the five-membered ring and hydroxyl six-membered ring of abiraterone, respectively (see Figure S4).

In addition, according to the mutagenesis studies,[8] F114 V mutant can cause combined hydroxylase/lyse deficiency, leading to very little hydroxylation or lyase enzymatic activity. Thus F114 is also suggested to be important for CYP17A1 specificity and may play key factors in orienting the ligands in the active site.

Similarly to these hydrophobic contributions, the van der Waals interactions of G301 and T306 are also much stronger than electrostatic effects. For R239, a combination of both electrostatic and van der Waals interactions acts to contribute

Table 4. Binding Free Energies (kcal mol^{-1}) and Its Components for wt17A1, Y201N, and E305G Mutants

system	ΔE_{ele}	ΔE_{vdw}	ΔG_{GB}	ΔG_{SASA}	$\Delta G_{MM\text{-}GB/SA}{}^a$	$-T\Delta S$	$\Delta G_{TOT}{}^b$
wt17A1	7.18 ± 1.19	−49.01 ± 2.94	21.65 ± 2.74	−5.38 ± 0.10	−25.56 ± 3.91	10.61 ± 0.95	−14.95 ± 1.91
Y201N	8.23 ± 1.14	−42.48 ± 3.55	22.15 ± 2.06	−3.32 ± 0.19	−15.42 ± 1.97	11.99 ± 1.08	−3.43 ± 1.44
E305G	9.71 ± 1.32	−42.84 ± 3.92	20.67 ± 3.03	−3.38 ± 0.22	−15.84 ± 1.72	13.60 ± 1.04	−2.24 ± 1.02

$^a \Delta G_{MM\text{-}GB/SA} = \Delta E_{ele} + \Delta E_{vdw} + \Delta G_{GB} + \Delta G_{SASA}$. $^b \Delta G_{TOT} = \Delta G_{MM\text{-}GB/SA} - T\Delta S$.

significant effects in the stabilization of ligand. It should be noted, E305 makes strongly favorable electrostatic interaction as well as favorable van der Waals contact, for a net contribution of about 1 kcal mol^{-1} for wt17A1 and Y201N mutant. However, for E305G mutant, G305 contributes much weaker to the affinity. In addition, the pronounced increase of nonpolar interaction ($\Delta G_{nonpolar} = \Delta G_{vdw} + \Delta G_{SASA}$) of I206 for E305G mutant compared with other two systems (−1.42, −0.98, and −1.49 kcal mol^{-1} for wt17A1, Y201N, and E305G, respectively) correlates well with the closer distance between I206 and abiraterone due to the extension of I206 side chain to the unfilled space adjacent to the mutational G305.

Overall, a large fraction of the binding affinity for these three systems can be attributed to a common set of interactions; the contributions of each interaction are detailed in Table 4. Consistent with previous analysis, the calculations exhibit the most profound change upon mutation. The binding free energy is decreased by 11.52 kcal mol^{-1} upon Y201N mutation and decreased by 12.71 kcal mol^{-1} upon E305G mutation, which are in accord with experimentally observed decreased enzymatic activities. Furthermore, the overall binding free energy changes are mainly attributed to nonpolar contributions, which are reasonable, since the hydrophobic residues constitute the tunnel bottleneck to control ligand access and form a hydrophobic cavity above the active site to play an indispensable role in the stabilization of ligands.

Unbinding Process along the Major Pathway by SMD Simulations and Energetic PMF Calculations. To estimate the effects of the mutations in terms of the energetic property between the enzyme and abiraterone, as well as the accessibility for ligand migrating along the tunnel systems hosted in three systems, the migration free energy profiles[42] were evaluated in Figure 8.

Twenty trajectories for each system were produced repeatedly to obtain the free energy profiles. Remarkably, abiraterone was pulled out of the heme active site along tunnel

Figure 8. PMF profile along the reaction coordinate for wt17A1, Y201N, and E305G mutants.

3 in both wt17A1 and Y201N, whereas the departure of the ligand was along tunnel S in E305G mutant (Figure S5). This result is in accordance with the suggestion of top ranked tunnels identified by CAVER. As shown in Figure 8, the energy changes in the course of abiraterone dissociation along major tunnel in each system are nearly 14.5 kcal mol^{-1}, 13.0 kcal mol^{-1}, and 11.5 kcal mol^{-1}, respectively. The shapes of wt17A1 and Y201N change linearly along tunnel 3, whereas the shape of E305G along tunnel S rapidly changes from 15 to 25 Å, and then the enhancing trend of energy slows down to change linearly from 25 to 40 Å. The PMF values of wt17A1 and Y201N differ by approximately 1.5 kcal mol^{-1}, whereas wt17A1 and E305 differ by nearly 3 kcal mol^{-1}. It can be inferred that the mutations at the entrances of different tunnels can both decrease the stability of ligand binding. Thus, the SMD simulations and the MM-GBSA calculations give a reasonable agreement with the experimental results and provide the probable explanation for the common catalysis deficiencies caused by these two mutations.

The Observed Local Structural Changes upon Single Point Mutations Are Directly Projected onto the Opening of Major Tunnels. The heterogeneities in conformational dynamics between wt17A1 and two mutants point out contradictive structural migrations by F and G helices. For Y201N mutant, the outward motion of G helix leads to an open conformation of the protein. By performing SMD simulations and CAVER analysis, tunnel 3 is inferred to be the major tunnel for ligand ingress and egress in both wt17A1 and Y201N mutant. From SASA and cross-correlation analysis, conformational changes of F, G helices are mainly attributed by the disruptions of HC1, which correlates well with the wider opening of tunnel 3. Thus it can be inferred that the open conformation favors the opening of tunnel 3 and thereby results in the more exposure of ligands to aqueous solution. For E305G mutant, hydrophobic interactions combined with the hydrogen bonds and salt bridges between F and G helices collectively cause the movements of G helix toward F helix direction and form the closed conformation. The structural compact of F and G helices is correlated with the narrower opening of tunnel 3, whereas tunnel S opens wider and ranks as the dominant pathway instead of tunnel 3, providing alternative route for ligands to enter the protein active site. In summary, we observed that both mutants show relatively more frequent opening of the respective major pathway (tunnel 3 for Y201N mutant and tunnel S for E305G mutant) and wider bottlenecks than the wild type protein, which results in the decrease of ligand binding affinity. Moreover, the MM-GBSA calculations and the SMD simulations give a reasonable agreement with the experimental results and provide evidence for previous conjecture that open/closed conformational changes induced by mutations correlate very well with the ligand binding affinity and enzymatic activity.

Overall, it is reasonable to propose that the decreased enzymatic activities caused by Y201N or E305G mutants, which is suggested to be associated with the less affinity of ligand
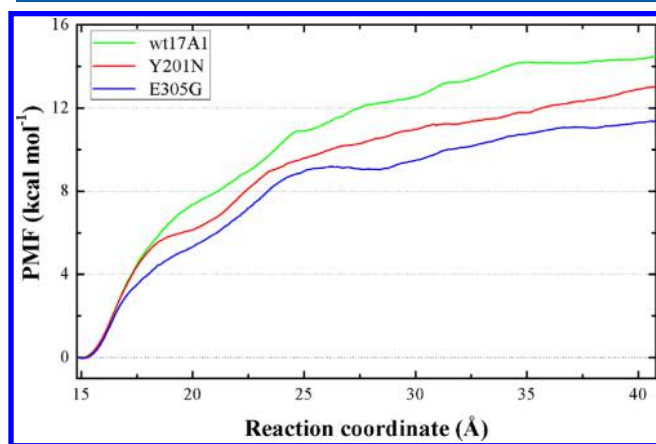
binding, may be due to the possible and not mutually exclusive mechanism: The observed local structural changes upon single point mutations are directly projected onto the opening of major pathway for ligand ingress and egress. The open conformation facilitates the wider opening of tunnel 3, which may be the major tunnel in both wt17A1 and Y210N. The closed conformation restricts the opening of tunnel 3 and favors the wider opening of tunnel S, which becomes the new major tunnel in E305G. The wider bottlenecks of these two major tunnels induced by the allostery may contribute to destabilize the ligand binding and thereby lead to the decreased enzymatic activity.

CONCLUSION

The application of MD simulations and SMD simulations has become indispensable in computational area of particular emphasis with regard to receptor−ligand interactions.[40,43] In this study, CAVER was performed to open up new possibilities for the study of important time evolution biochemical phenomena of the transport pathways and to identify the structural basis of pathway gating mechanism combined with SMD simulations.

Our present study is performed based on the existent CYP17A1 abiraterone-bound crystal structure and the ample experimental mutagenesis data. We have investigated the atomic-level structural variations and its two mutants of experimental interests (Y201N and E305G) to understand the molecular origin for the decreased enzymatic activity. Although the overall protein topologies are fairly conserved between wt17A1 and two mutants, the heterogeneous variations in local fluctuations are observed upon mutations. The observed local structural changes upon single point mutations are directly projected onto the opening of major pathway for ligand ingress and egress. Both mutations cause the decrease of ligand binding affinity, mainly attributed to the wider opening of their respective major tunnels and the more exposure of ligand to the aqueous solution. The underlying molecular mechanism is considered to be associated with the closer distances of hydrophobic residues or the disruption of the HC1. Moreover, the MM-GBSA calculations and the SMD simulations give a reasonable agreement with the experimental results and provide evidence for previous conjecture that conformational changes induced by mutations correlate very well with the ligand binding affinity and enzymatic activity. The decomposition analysis of binding free energy in connection with tunnel bottleneck analysis highlights the fact that the changes in binding free energy mainly originate from hydrophobic residues with nonpolar contributions.

Based on our results, we present such "access mechanism" which encapsulates the effects of mutations on the changes in both structural flexibility and tunnel dynamics. Similar findings have gained some success, which explains the long-rang effects of peripheral mutation on CYP1A2.[41] The current study highlights the potential application of this mechanism to a wide range of other proteins including CYP proteins whose activities depend on access channels.

In summary, our work provides detailed atomistic insight into the effects on the conformational changes and tunnel dynamics upon single point mutations in CYP17A1. The MD simulation results combined with PMF calculations render the structural motif and molecular origin to rationalize the experimentally observed decrease of enzymatic activity by the single point mutation. The knowledge of ligand binding characteristics and key residues contributions could guide future experimental and computational work on CYPs so that desirable changes in their enzymatic activities may be achieved. Our present study provides important insights into the structure−function relationships of proteins, which could contribute to further understanding about 17-hydroxylase deficiencies and may also improve our understanding of polycystic ovary disease.

ASSOCIATED CONTENT

Ⓢ Supporting Information

Structural characteristics of crucial residues and their decomposition binding free energies. This material is available free of charge via the Internet at http://pubs.acs.org.

AUTHOR INFORMATION

Corresponding Author

*E-mail: zhengqc@jlu.edu.cn (Q.-C.Z.), zhanghx@mail.jlu.edu.cn (H.-X.Z.).

Notes

The authors declare no competing financial interest.

ACKNOWLEDGMENTS

REFERENCES

(1) Meng, X. Y.; Zheng, Q. C.; Zhang, H. X. A comparative analysis of binding sites between mouse CYP2C38 and CYP2C39 based on homology modeling, molecular dynamics simulation and docking studies. *BBA, Biochim. Biophys. Acta, Proteins Proteomics* **2009**, *1794*, 1066−1072.

(2) Yamashita, F.; Feng, C.; Yoshida, S.; Itoh, T.; Hashida, M. Automated information extraction and structure-activity relationship analysis of cytochrome P450 substrates. *J. Chem. Inf. Model.* **2011**, *51*, 378−385.

(3) Cong, S.; Ma, X.-T.; Li, Y.-X.; Wang, J.-F. Structural basis for the mutation-induced dysfunction of human CYP2J2: A computational study. *J. Chem. Inf. Model.* **2013**, *53*, 1350−1357.

(4) Lorbek, G.; Lewinska, M.; Rozman, D. Cytochrome P450s in the synthesis of cholesterol and bile acids−from mouse models to human diseases. *FEBS J.* **2012**, *279*, 1516−1533.

(5) Saenz-Méndez, P.; Elmabsout, A. A.; Sävenstrand, H.; Awadalla, M. K. A.; Strid, Å.; Sirsjö, A.; Eriksson, L. A. Homology models of human all-trans retinoic acid metabolizing enzymes CYP26B1 and CYP26B1 spliced variant. *J. Chem. Inf. Model.* **2012**, *52*, 2631−2637.

(6) Park, H.; Lee, S.; Suh, J. Structural and dynamical basis of broad substrate specificity, catalytic mechanism, and inhibition of cytochrome P450 3A4. *J. Am. Chem. Soc.* **2005**, *127*, 13634−13642.

(7) Tyzack, J. D.; Williamson, M. J.; Torella, R.; Glen, R. C. Prediction of cytochrome P450 xenobiotic metabolism: Tethered docking and reactivity derived from ligand molecular orbital analysis. *J. Chem. Inf. Model.* **2013**, *53*, 1294−1305.

(8) DeVore, N. M.; Scott, E. E. Structures of cytochrome P450 17A1 with prostate cancer drugs abiraterone and TOK-001. *Nature* **2012**, *482*, 116−119.

(9) Swart, A. C.; Storbeck, K. H.; Swart, P. A single amino acid residue, Ala 105, confers 16α-hydroxylase activity to human cytochrome P450 17α-hydroxylase/17, 20 lyase. *J. Steroid Biochem. Mol. Biol.* **2010**, *119*, 112−120.

(10) Patocs, A.; Liko, I.; Varga, I.; Gergics, P.; Boros, A.; Futo, L.; Kun, I.; Bertalan, R.; Toth, S.; Pazmany, T.; Toth, M.; Szucs, N.; Horanyi, J.; Glaz, E.; Racz, K. Novel mutation of the CYP17 gene in two unrelated patients with combined 17 alpha-hydroxylase/17,20-lyase deficiency: Demonstration of absent enzyme activity by

expressing the mutant CYP17 gene and by three-dimensional modeling. *J. Steroid Biochem. Mol. Biol.* **2005**, *97*, 257−265.

(11) van den Akker, E. L. T.; Koper, J. W.; Boehmer, A. L. M.; Themmen, A. P. N.; Verhoef-Post, M.; Timmerman, M. A.; Otten, B. J.; Drop, S. L. S.; De Jong, F. H. Differential inhibition of 17α-hydroxylase and 17, 20-lyase activities by three novel missense CYP17 mutations identified in patients with P450c17 deficiency. *J. Clin. Endocrinol. Metab.* **2002**, *87*, 5714−5721.

(12) Di Cerbo, A.; Biason-Lauber, A.; Savino, M.; Piemontese, M. R.; Di Giorgio, A.; Perona, M.; Savoia, A. Combined 17α-hydroxylase/17, 20-lyase deficiency caused by Phe93Cys mutation in the CYP17 gene. *J. Clin. Endocrinol. Metab.* **2002**, *87*, 898−905.

(13) Attard, G.; Reid, A. H. M.; Yap, T. A.; Raynaud, F.; Dowsett, M.; Settatree, S.; Barrett, M.; Parker, C.; Martins, V.; Folkerd, E.; Clark, J.; Cooper, C. S.; Kaye, S. B.; Dearnaley, D.; Lee, G.; de Bono, J. S. Phase I clinical trial of a selective inhibitor of CYP17, abiraterone acetate, confirms that castration-resistant prostate cancer commonly remains hormone driven. *J. Clin. Oncol.* **2008**, *26*, 4563−4571.

(14) Attard, G.; Reid, A. H. M.; A'Hern, R.; Parker, C.; Oommen, N. B.; Folkerd, E.; Messiou, C.; Molife, L. R.; Maier, G.; Thompson, E.; Olmos, D.; Sinha, R.; Lee, G.; Dowsett, M.; Kaye, S. B.; Dearnaley, D.; Kheoh, T.; Molina, A.; de Bono, J. S. Selective inhibition of CYP17 with abiraterone acetate is highly active in the treatment of castration-resistant prostate cancer. *J. Clin. Oncol.* **2009**, *27*, 3742−3748.

(15) Chong, S.-H.; Lee, C.; Kang, G.; Park, M.; Ham, S. Structural and thermodynamic investigations on the aggregation and folding of acylphosphatase by molecular dynamics simulations and solvation free energy analysis. *J. Am. Chem. Soc.* **2011**, *133*, 7075−7083.

(16) Fukunishi, H.; Yagi, H.; Kamijo, K.; Shimada, J. Role of a mutated residue at the entrance of the substrate access channel in cytochrome P450 engineered for vitamin D-3 hydroxylation activity. *Biochemistry* **2011**, *50*, 8302−8310.

(17) Discovery Studio, Version 2.5; Accelrys Inc.: San Diego, CA, 2007.

(18) Case, D.; Darden, T.; Cheatham, T., III; Simmerling, C.; Wang, J.; Duke, R.; Luo, R.; Walker, R.; Zhang, W.; Merz, K. *AMBER 11*; University of California, San Francisco: 2010; p 142.

(19) Sun, H.; Li, Y.; Li, D.; Hou, T. Insight into crizotinib resistance mechanisms caused by three mutations in ALK tyrosine kinase using free energy calculation approaches. *J. Chem. Inf. Model.* **2013**, *53*, 2376−2389.

(20) Frisch, M.; Trucks, G. W.; Schlegel, H.; Scuseria, G.; Robb, M.; Cheeseman, J.; Scalmani, G.; Barone, V.; Mennucci, B.; Petersson, G.; Nakatsuji, H. *Gaussian 09 2009*; Gaussian, Inc.: Wallingford, CT, 2009.

(21) Shahrokh, K.; Orendt, A.; Yost, G. S.; Cheatham, T. E., III Quantum mechanically derived AMBER-compatible heme parameters for various states of the cytochrome P450 catalytic cycle. *J. Comput. Chem.* **2012**, *33*, 119−133.

(22) Rydberg, P.; Olsen, L.; Norrby, P. O.; Ryde, U. General transition-state force field for cytochrome P450 hydroxylation. *J. Chem. Theory Comput.* **2007**, *3*, 1765−1773.

(23) Li, D.; Wang, Y.; Han, K.; Zhan, C. G. Fundamental reaction pathways for cytochrome P450-catalyzed 5′-hydroxylation and N-demethylation of nicotine. *J. Phys. Chem. B* **2010**, *114*, 9023−9030.

(24) Hornak, V.; Abel, R.; Okur, A.; Strockbine, B.; Roitberg, A.; Simmerling, C. Comparison of multiple Amber force fields and development of improved protein backbone parameters. *Proteins: Struct., Funct., Bioinf.* **2006**, *65*, 712−725.

(25) DeLano, W. L. The PyMOL Molecular Graphics System, Version 1.1; Schroinger LLC: 2002. http://www.pymol.org (accessed November 11, 2013).

(26) Pettersen, E. F.; Goddard, T. D.; Huang, C. C.; Couch, G. S.; Greenblatt, D. M.; Meng, E. C.; Ferrin, T. E. UCSF Chimera—a visualization system for exploratory research and analysis. *J. Comput. Chem.* **2004**, *25*, 1605−1612.

(27) Swanson, J. M. J.; Henchman, R. H.; McCammon, J. A. Revisiting free energy calculations: a theoretical connection to MM/PBSA and direct calculation of the association free energy. *Biophys. J.* **2004**, *86*, 67−74.

(28) Hou, T. J.; Zhang, W.; Case, D. A.; Wang, W. Characterization of domain-peptide interaction interface: A case study on the amphiphysin-1 SH3 domain. *J. Mol. Biol.* **2008**, *376*, 1201−1214.

(29) Petřek, M.; Otyepka, M.; Banáš, P.; Košinová, P.; Koča, J.; Damborský, J. CAVER: A new tool to explore routes from protein clefts, pockets and cavities. *BMC Bioinf.* **2006**, *7*, 316.

(30) Chovancova, E.; Pavelka, A.; Benes, P.; Strnad, O.; Brezovsky, J.; Kozlikova, B.; Gora, A.; Sustr, V.; Klvana, M.; Medek, P. CAVER 3.0: A tool for the analysis of transport pathways in dynamic protein structures. *PLoS Comput. Biol.* **2012**, *8*, e1002708.

(31) Fukunishi, H.; Yagi, H.; Kamijo, K. i.; Shimada, J. Role of a mutated residue at the entrance of the substrate access channel in cytochrome P450 engineered for vitamin D3 hydroxylation activity. *Biochemistry* **2011**, *50*, 8302−8310.

(32) Park, S.; Khalili-Araghi, F.; Tajkhorshid, E.; Schulten, K. Free energy calculation from steered molecular dynamics simulations using Jarzynski's equality. *J. Chem. Phys.* **2003**, *119*, 3559.

(33) Jarzynski, C. Nonequilibrium equality for free energy differences. *Phys. Rev. Lett.* **1997**, *78*, 2690.

(34) Speck, T.; Seifert, U. Distribution of work in isothermal nonequilibrium processes. *Phys. Rev. E* **2004**, *70*, 066112.

(35) Calvaresi, M.; Hoefinger, S.; Zerbetto, F. Probing the structure of lysozyme−carbon−nanotube hybrids with molecular dynamics. *Chem.—Eur. J.* **2012**, *18*, 4308−4313.

(36) Chen, L.; Zhang, J.-L.; Yu, L.-Y.; Zheng, Q.-C.; Chu, W.-T.; Xue, Q.; Zhang, H.-X.; Sun, C.-C. Influence of hyperthermophilic protein Cren7 on the stability and conformation of DNA: Insights from molecular dynamics simulation and free energy analysis. *J. Phys. Chem. B* **2012**, *116*, 12415−12425.

(37) Cojocaru, V.; Winn, P. J.; Wade, R. C. The ins and outs of cytochrome P450s. *Biochim. Biophys. Acta* **2007**, *1770*, 390.

(38) Schleinkofer, K.; Sudarko, P. J. W.; Lüdemann, S. K.; Wade, R. C. Do mammalian cytochrome P450s show multiple ligand access pathways and ligand channelling? *EMBO Rep.* **2005**, *6*, 584−589.

(39) Haines, D. C.; Tomchick, D. R.; Machius, M.; Peterson, J. A. Pivotal role of water in the mechanism of P450BM-3. *Biochemistry* **2001**, *40*, 13456−13465.

(40) Cui, Y. L.; Zhang, J. L.; Zheng, Q. C.; Niu, R. J.; Xu, Y.; Zhang, H. X.; Sun, C. C. Structural and dynamic basis of human cytochrome P450 7B1: A survey of substrate selectivity and major active site access channels. *Chem.—Eur. J.* **2013**, *19*, 549−557.

(41) Zhang, T.; Liu, L. A.; Lewis, D. F.; Wei, D.-Q. Long-range effects of a peripheral mutation on the enzymatic activity of cytochrome P450 1A2. *J. Chem. Inf. Model.* **2011**, *51*, 1336−1346.

(42) Zhang, J.-L.; Zheng, Q.-C.; Li, Z.-Q.; Zhang, H.-X. How does (E)-2-(acetamidomethylene) succinate bind to its hydrolase? From the binding process to the final result. *PLoS One* **2013**, *8*, e53811.

(43) Xue, Q.; Zhang, J.-L.; Zheng, Q.-C.; Cui, Y.-L.; Chen, L.; Chu, W.-T.; Zhang, H.-X. Exploring the molecular basis of dsRNA recognition by Mss116p using molecular dynamics simulations and free energy calculations. *Langmuir* **2013**, *29*, 11135−11144.